ICARUS 113, 267–276 (1995)

Titan's Stratospheric Temperature Asymmetry: A Radiative Origin?

BRUNO BÉZARD AND ATHÉNA COUSTENIS

Département de Recherche Spatiale, Observatoire de Paris (Section de Meudon), 92195 Meudon Principal Cedex, France
E-mail: bezard@obspm.fr

AND

CHRISTOPHER P. MCKAY

Space Science Division, NASA Ames Research Center, Moffett Field, California 94035

Received December 14, 1993; revised August 22, 1994

During the 1981 *Voyager* encounter, Titan's stratosphere exhibited a large thermal asymmetry, with high northern latitudes being colder than comparable southern latitudes. Given the short radiative time constant, this asymmetry would not be expected at the season of the *Voyager* observations (spring equinox), if the infrared and solar opacity sources were distributed symmetrically. We have investigated the radiative budget of Titan's stratosphere, using two selections of *Voyager* IRIS spectra recorded at symmetric northern and southern latitudes. In the region 0.1–1 mbar, temperatures are 7 K colder at 50°N than at 53°S and the difference reaches ~13 K at 5 mbar. On the other hand, the northern region is strongly enriched in nitriles and hydrocarbons, and the haze optical depth derived from the continuum emission between 8 and 15 μm is twice as large as in the south. Cooling rate profiles have been computed at the two locations, using the gas and haze abundances derived from the IRIS measurements. We find that, despite lower temperatures, the cooling rate profiles in the pressure range 0.15–5 mbar are 20 to 40% larger in the north than in the south, because of the enhanced concentrations of infrared radiators. Because the northern hemisphere appears darker than the southern one in the *Voyager* images, enhanced solar heating is also expected to take place at 50°N. Solar heating rate profiles have been calculated, with two different assumptions on the origin of the hemispheric asymmetry. In the most likely case where it results from a variation in the absorbance of the haze material, the heating rates are found to be 12–15% larger at the northern location than at the southern one, a smaller increase than that in the cooling rates. If the lower albedo in the north results from an increase in the particle number density, a 55 to 75% difference is found for the pressure range 0.15–5 mbar, thus larger than that calculated for the cooling rates. Considering the uncertainties in the haze model, dynamical heat transport may significantly contribute to the meridional temperature gradients observed in the stratosphere. On the other hand, the latitudinal variation in gas and haze composition may be sufficient to explain the entire temperature asymmetry observed, without invoking a lag in the thermal response of the atmosphere due to dynamical inertia.

1. INTRODUCTION

Infrared observations by the *Voyager* 1 spacecraft indicate that the thermal structure of Titan's stratosphere is asymmetric about the equator. This asymmetry was first pointed out by Flasar *et al.* (1981) from an investigation of the meridional variation of the thermal emission in the υ_4 band of methane at 7.7 μm recorded with the infrared spectrometer aboard *Voyager* 1 (IRIS). Flasar and Conrath (1990) retrieved temperatures in the region 1 to 0.4 mbar by inverting the IRIS radiances in the CH_4 υ_4 band. They confirmed that the northern hemisphere was significantly colder than the southern one and found temperature differences near 55°N and S latitude of 4 and 8 K at 1 and 0.4 mbar respectively. The same meridional structure was recently derived by Coustenis and Bézard (1994) from fitting of the υ_4 band of methane for different selections of IRIS spectra.

This north-to-south asymmetry is not expected on the basis of radiative equilibrium, provided that the opacity sources responsible for cooling and heating the stratosphere are symmetric with respect to the equator. The *Voyager* spacecraft observed Titan in 1980 at its northern spring equinox, so that the insolation pattern was then symmetric. Radiative time constants in the region 1-mbar are much shorter than a Titanian year (Flasar *et al.* 1981), so that the radiative response of the atmosphere at the observed levels should not significantly lag behind the solar forcing. In other words, the thermal structure at the *Voyager* encounter should be close to radiative equilibrium for the solar forcing at the same epoch, and thus be symmetric about the equator.

0019-1035/95 $6.00

Flasar and Conrath (1990) proposed that the observed temperature asymmetry was due to a phase lag in the response of the atmosphere to the insolation linked to dynamical motions. They pointed out that seasonal changes in the temperature structure must be accompanied by changes in angular momentum transport in order to maintain cyclostrophic equilibrium. Using a simple zonally symmetric model, they found that the time scale for redistributing the axial angular momentum was comparable to a Titan season. The phase lag so-introduced could then, at least qualitatively, account for the observed asymmetry in the temperature field which would thus be representative of northern winter solstice conditions of insolation.

However, as noted by Flasar and Conrath (1990), their model relies on the assumption that the distribution of opacity sources is symmetric with latitude. *Voyager* observations tell us that this is not the case. IRIS measurements show that high northern latitudes are strongly enriched in nitriles and some hydrocarbons (Coustenis and Bézard 1994). These gases exhibit strong rovibrational bands in the thermal infrared and are thus efficient radiators in the stratosphere. Similarly, analysis of IRIS spectra show that the continuum opacity due to stratospheric hazes is enhanced in the northern hemisphere (Coustenis and Bézard 1994). Larger gas and haze opacities tend to more efficiently cool the stratosphere and thus lower radiative equilibrium temperatures at northern latitudes. On the other hand, the northern hemisphere of Titan appears darker than the southern one in *Voyager* images (Sromovsky *et al.* 1981). More solar energy is thus absorbed in the north, resulting in larger heating rates. This effect compensates, at least partly, for the higher cooling rates due to the enrichment in infrared emittors (gas and haze).

This paper investigates the possibility that the latitudinal variations in composition contribute substantially to the observed temperature asymmetry. The north-to-south asymmetries observed by *Voyager* in terms of temperature, gas mixing ratios, and haze structure are first reviewed in Section 2. Using radiative transfer models, we calculate in Sections 3 and 4 the stratospheric cooling and heating rates at a reference latitude (53°S). We show that radiative cooling is essentially balanced by solar heating in the atmospheric region probed by the IRIS measurements, implying that radiative equilibrium prevails in this region. We then calculate the cooling and heating rates at a symmetric latitude (50°N) and see how they are affected by the compositional variations between the two locations. We thus assess if these variations are large enough to account for the observed temperature differences under the assumption of radiative equilibrium. Section 5 discusses the results of our calculations and presents the conclusions of this study.

2. NORTH-TO-SOUTH ASYMMETRY

By comparing synthetic calculations to *Voyager* 1 IRIS data, Coustenis and Bézard (1994) investigated the variations in the temperature field and in the distribution of opacity sources (gases and haze) in nine different locations on Titan's disk. We will consider here two of these latitudes symmetric with respect to the equator. The observational data set consists of two selections performed in the initial 300 usable IRIS-spectra lot, near 50°N and 53°S, in which the spectra included were coadded. The two selections contain 30 and 27 spectra and correspond to a mean airmass of 2.0 and 1.5 for the north and the south respectively. They are explicitly described in Coustenis and Bézard (1994) (Samples E and I for the 50°N and 53°S regions respectively) and are shown in Fig. 1. As discussed below, the differences in the strengths of the emission features from the two selections are indicators of the large meridional variations in temperature and composition existing in the stratosphere.

The method and spectroscopic line parameters used to analyze the spectra have been extensively described in Coustenis *et al.* (1989) and updated in Coustenis and Bézard (1994). We summarize below the results of Coustenis and Bézard's analysis relevant to the spectral selections at 50°N and 53°S.

a. Temperature

For each selection, the temperature profile was inferred from a three-step procedure: in the troposphere and lower stratosphere (0–65 km), due to lack of information on temperature variations with latitude, we adopted for all latitudes the nominal temperature profile derived by Lellouch *et al.* (1989) from a reanalysis of the radio-occultation (RSS) *Voyager* data near Titan's equator. The analysis of the emission observed in the υ_4 methane band at 7.7 μm yields direct indications on the stratospheric temperature in the altitude range 120–350 km approximately. A uniform stratospheric methane mole fraction of 2% was assumed in the radiative transfer calculations. The upper part of the atmosphere was modeled by Yelle (1991), and we used the shape of the temperature profile found in his model J for the region above 350 km.

The two temperature profiles derived for the 50°N and 53°S samples are displayed in Fig. 2. Based on the assumption that methane is uniformly mixed with latitude, the northern profile is significantly colder than the southern one in the region probed by the IRIS measurements. This can readily be seen from the radiances in the CH_4 band which are lower in the north despite a larger emission angle (Fig. 1). The southern profile is 7 K warmer than the northern above the 1-mbar level. Below, the northern profile becomes steeper and the difference reaches ~13 K at 5 mbar. Maximum sensitivity of the outgoing radi-

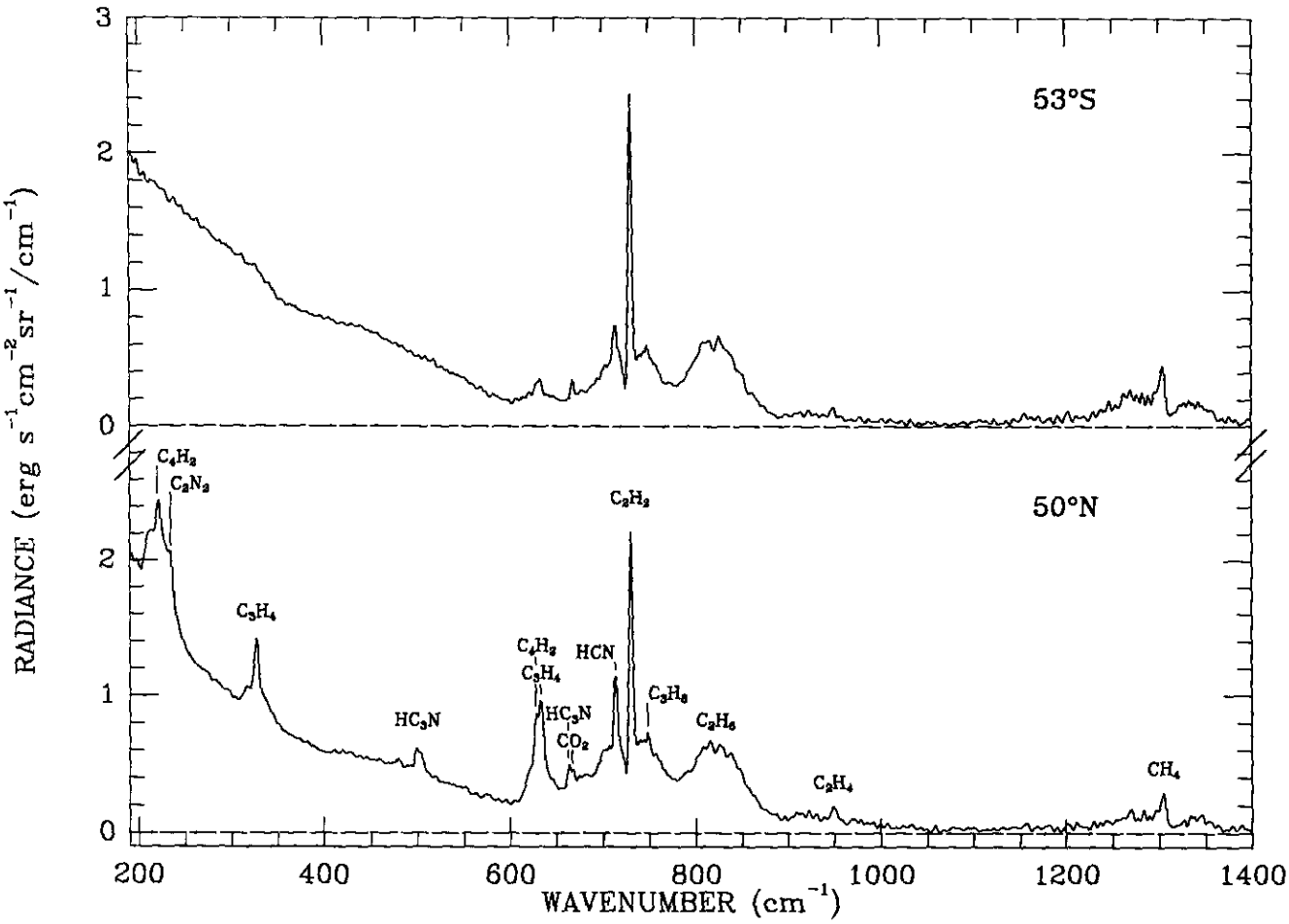

FIG. 1. Average spectra of two homogeneous selections of 30 and 27 individual *Voyager* IRIS spectra recorded near latitudes of 53°S and 50°N. Stratospheric temperatures are colder in the north, as revealed by the lower intensity of the methane band near 1304 cm^{-1}. On the other hand, molecular species other than methane and carbon dioxide show enhanced concentrations at northern latitudes.

ance to temperature occurs near 0.4 mbar in the Q-branch of the methane band (1304 cm^{-1}), and near 1 mbar in the P- and R-branches. At half maximum, the weighting functions extend from 0.15 to 1.5 mbar at 1304 cm^{-1}, and from 0.2 to 5 mbar in the P-branch at 1270 cm^{-1}. The formal temperature uncertainty due to the 1 SD noise is about 0.8 K (1.0 K) at 0.4 mbar and 0.6 K (0.8 K) at 1 mbar for the southern (northern) selection. These results are in good agreement with those of Flasar and Conrath (1990), with some slight differences probably due to different upper boundary conditions in the profiles.

Attention should be drawn however to the fact that the derived temperature asymmetry relies on the assumption that methane is uniformly mixed with latitude in the stratosphere. Conversely, the possibility that the observed asymmetry in the CH_4 emission could be due to horizontal variations in the methane mole fraction cannot be discarded. We found however that a decrease by an order of magnitude in the CH_4 mole fraction would be required to reproduce the υ_4-band emission at high northern latitudes, using the same temperature profile as in the south. Such a large latitudinal variation seems unlikely. Methane originates from the surface of Titan, and its abundance in the upper part of the troposphere is limited by saturation. The stratospheric CH_4 mole fraction is thus likely to be regulated by the temperature at the cold trap near the tropopause. A factor of 10 depletion at northern latitudes would imply a temperature $\approx$10 K lower at the cold trap, while *Voyager* infrared measurements near 200 cm^{-1} only indicate a $\approx$1 K meridional contrast (Flasar *et al.* 1981). Dynamical motions would furthermore tend to reduce any meridional composition gradient. For these reasons, we think that *Voyager* observations point out to a real asymmetry in the temperature field of Titan's stratosphere.

b. Haze Opacity

The continuum emission present in the IRIS spectra (Fig. 1) originates from two basic sources: (1) collision-

induced absorption from the various N_2–CH_4–H_2 combinations, and (2) opacity due to the tropospheric clouds and stratospheric aerosols. The cloud/haze model used in Coustenis and Bézard consists of a tropospheric cloud located between 20 and 40 km, and a semi-infinite haze layer uniformly mixed with gas above the tropopause (40 km). Only particle absorption is considered; scattering processes are neglected, which is justified given the small size of the haze particles compared to thermal infrared wavelengths (Rages and Pollack 1980). The stratospheric haze is by far the dominant source of continuum opacity at wavenumbers higher than 600 cm^{-1}. By fitting the observed spectra at selected frequencies, free of emission from molecular bands, the haze optical depth can be retrieved for each spectral selection between ~600 and 1100 cm^{-1}. In this range, the haze optical depth in the north was found to be consistently 2.2 ± 0.3 times that for the southern selection. Because the haze particles are Rayleigh absorbers, this enhancement could result from a similar increase either in the particle column density or in the absorbance of the particle material.

Below 600 cm^{-1}, both tropospheric and stratospheric layers contribute to the continuum emission. The contributions from the stratospheric haze and the methane cloud cannot be disentangled due to the lack of limb-darkening information or limb-viewing observations at the two investigated latitudes. Coustenis and Bézard (1994) fitted the continuum using some spectral information on the haze opacity derived by Samuelson and Mayo (1991) for the north polar and equatorial regions. Note that the parameters chosen to reproduce the continuum do not affect the determination of the gaseous abundances from the molecular emission bands.

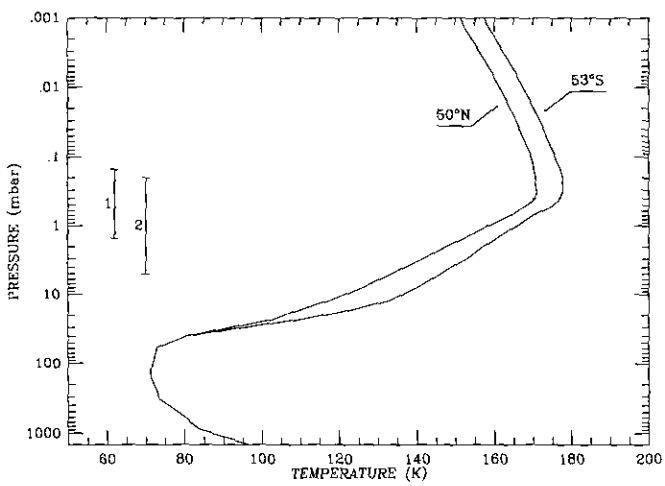

FIG. 2. Temperature profiles derived from the best fitting of the υ_4 band of methane (after Coustenis and Bézard (1994)). The northern profile is ~7 K colder than the southern one above 1 mbar. The difference increases with depth, reaching ~13 K at 5 mbar. The approximate pressure ranges probed at 1304 cm^{-1} (1) and in the P-branch (2) are indicated. The formal error bars on temperature proceeding from the 1 SD noise in the two selections are plotted on the profiles at 0.4 and 1 mbar.

TABLE I
Stratospheric Composition of Titan[a]

Molecule	Band center (cm^{-1})	Mixing ratio 50°N	Mixing ratio 53°S	North/South ratio
CH_4	1304	1.9×10^{-2}[b]	1.9×10^{-2}[b]	1
C_2H_2	729	5.5×10^{-6}	2.5×10^{-6}	2.2
C_2H_4	949	1×10^{-6}	1.5×10^{-7}	7
C_2H_6	822	2.2×10^{-5}	1.3×10^{-5}	1.7
C_3H_4	327, 633	3.3×10^{-8}	3.5×10^{-9}	9
C_3H_8	748	8×10^{-7}	4×10^{-7}	2
C_4H_2	220, 628	1.5×10^{-8}	1.0×10^{-9}	15
HCN	713	1.1×10^{-6}	4.7×10^{-8}	22
C_2N_2	234	1.5×10^{-8}	$<1.5 \times 10^{-9}$	>10
HC_3N	500, 663	2.3×10^{-8}	$<1.5 \times 10^{-9}$	>15
CO_2	667	1.0×10^{-8}	1.3×10^{-8}	0.8
Haze (τ/τ_0)[c]	>600	1.8	0.8	2.2

[a] After Coustenis and Bézard (1994).
[b] Assumed.
[c] Optical depths ratioed to the equatorial values τ_0.

c. *Gas Abundances*

Mixing ratios of the infrared absorbers were derived from the best fitting of their emission bands in the IRIS spectra (Coustenis and Bézard 1994). In the calculations, the gas mixing ratios were assumed to be constant with altitude above their condensation levels. The gas composition derived for the two selections is given in Table I. The formal uncertainty on the concentrations due to noise only (1 SD) varies from 5 to 30% depending on the intensity of the emission features (e.g., Table II of Coustenis *et al.* 1989). A moderate south-to-north twofold enhancement is found for the most abundant hydrocarbons (C_2H_6, C_2H_2, C_3H_8) after CH_4. This enhancement is actually only marginally significant, considering all systematic uncertainties (particularly those attached to the temperature profile determinations) involved in the abundance retrievals. All other gases, besides CO_2, show huge enhancements at high northern latitudes. This can directly be seen in the IRIS measurements themselves (Fig. 1), where the emission features from these gases are much more pronounced in the northern spectrum, while the emission in the υ_4 band of methane, probing stratospheric temperatures, is weaker.

3. COOLING RATE CALCULATIONS

The cooling rate at a given pressure level p is defined as

$$K_c = \frac{mg}{C_p} \times \frac{dF_{ir}}{dp}, \quad (1)$$

where F_{ir} denotes the net upward thermal flux, mg is the mean molecular weight, and C_p the mean molar specific heat. In the absence of scattering, F_{ir} is given by

$$F_{ir} = \int_0^\infty 2\pi \left[\int_{\tau_\sigma}^\infty B_\sigma(T) E_2(t_\sigma - \tau_\sigma) dt_\sigma - \int_0^{\tau_\sigma} B_\sigma(T) E_2(\tau_\sigma - t_\sigma) dt_\sigma \right] d\sigma, \quad (2)$$

where τ_σ is optical depth at pressure level p and wavenumber σ, $B_\sigma(T)$ is the Planck radiance at temperature T and wavenumber σ, and E_2 is the second-order exponential integral.

For a given atmospheric model (temperature profile, gas and particle vertical distribution), the net thermal flux was calculated from Eq. (2), with the integration performed from 0 to 1400 cm^{-1}. This spectral region ($\lambda > 7$ μm) essentially covers all the thermal emission from Titan's atmosphere. Monochromatic opacities (t_σ) were computed on an 80-level grid extending from the ground up to 550 km, using a multilayer line-by-line radiative transfer code.

Spectroscopic line parameters used to calculate gaseous opacities are the same as in Coustenis and Bézard (1994). N_2–N_2, N_2–CH_4, and N_2–H_2 collision-induced opacity was modeled according to Courtin (1988). In the stratosphere, the gas mixing ratios, assumed to be constant with altitude above their condensation levels, were taken from Table I.

The cloud/haze model, summarized in Section 2, is the same as in Coustenis and Bézard (1994). The optical depth of the stratospheric haze (τ) at wavenumbers greater than 600 cm^{-1} comes from direct fitting of the continuum in the IRIS selections, as discussed in the previous section. In the region 250 to 600 cm^{-1}, the *spectral dependence* of the stratospheric haze opacity given by Samuelson and Mayo (1991) was used, along with our value for τ at 600 cm^{-1} as a reference point. For the southern selection, Samuelson and Mayo's results relative to the equatorial region were considered. Our nominal haze model for the 50°N region (H_{N1}) makes use of the spectral dependence derived by these authors from an IRIS limb-viewing sequence near 70°N. Because of the unknown actual spectral dependence of τ for $\sigma < 600$ cm^{-1} at the two investigated latitudes, we also consider an additional case (H_{N2}) where the haze opacity in the north has the same spectral dependence as that retained for the southern region (H_S). In this case, the factor of 2.2 enhancement in the north found at high wavenumbers holds over the whole IRIS spectral range. For $\sigma < 250$ cm^{-1}, we assumed a linear decrease of the optical depth with wavenumber. This gross assumption has negligible effect on the calculated cooling rates as, in our model, less than 2% of the total cooling rate originates from the haze opacity in the region 0–250 cm^{-1} at 1 mbar and above.

It is worth noting that the gas concentrations and haze extinction derived from IRIS measurements are mostly relevant to the region 1 to 20 mbar (see, e.g., the weighting functions in Fig. 11 of Coustenis *et al.* 1989). On the other hand, the temperature profile is best determined in the range 0.1–5 mbar (e.g., Fig. 1 of Flasar and Conrath 1990). Photochemical models (Yung *et al.* 1984) predict that the concentrations of nitriles and most hydrocarbons (except CH_4) increase with height in the stratosphere. *Voyager* data near 70°N actually indicate that this is the case, at least for nitriles and C_3H_4 (Coustenis *et al.* 1991). The cooling rates in the range 0.1–5 mbar would then be underestimated to some extent by our calculations. Similarly, although microphysical haze models by Toon *et al.* (1992) do predict that the haze is uniformly mixed with gas in the stratosphere as we assumed, there is no observational evidence that this is the case. It introduces further uncertainty in the cooling rates calculated ~2 scale heights above the region from which the bulk of the haze emission originates. However, this potential problem is probably not a major limitation to our study as we are chiefly interested in a comparison between northern and southern latitudes, rather than in the absolute values of the cooling rates.

We have then calculated the cooling rate profiles at latitudes of 50°N and 53°S, using the atmospheric models in Table I. The north and south temperature models are constrained by the IRIS observations only in the range ~0.15–5 mbar so that the cooling rate profiles are highly uncertain outside of this pressure range. We will hereafter only consider the results of the calculations pertaining to the two vertical regions around 0.4 and 1 mbar probed by the CH_4 ν_4-band emission (regions 1 and 2 indicated in Figs. 2–5).

Figure 3 shows the cooling rate profile at 53°S plotted against the heating rate profile for the same region. The latter was calculated from the nominal haze model of McKay *et al.* (1989), as described in Section 4. As expected, radiative cooling is approximately balanced by solar heating in the atmospheric regions of interest: averaged over the mbar interval 0.15–1.5 (Region 1), the cooling rate is ≈3% larger than the heating rate, while it is ≈15% lower in the region 0.2–5 mbar (Region 2). As discussed in Section 5, this good agreement supports the generally recognized idea that the thermal structure of the stratosphere is globally controlled by radiative equilibrium (Samuelson 1983, McKay *et al.* 1989). On the other hand, the calculated heating and cooling rates are obvi-

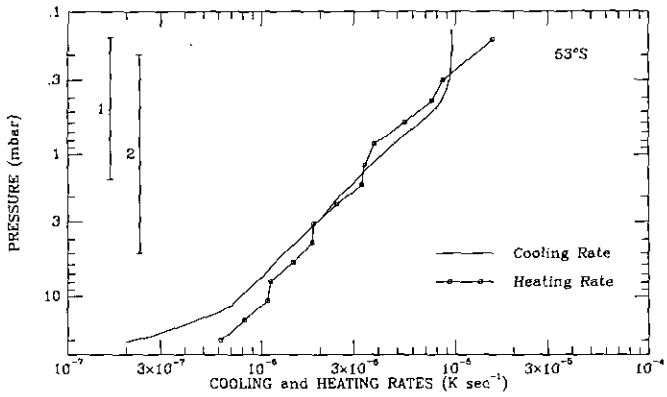

FIG. 3. Cooling and heating rate profiles at 53°S. Cooling rates were calculated using an atmospheric model which reproduces the *Voyager* infrared spectrum at this location (Fig. 2 and Table I). Heating rate calculations were carried out with the nominal haze model of McKay *et al.* (1989) with the particle number density multiplied by 0.8 to correct for the reduced haze opacity at this latitude (Table I).

ously most sensitive to uncertainties in the atmospheric model (such as those in the vertical distributions of minor gases and particles) so that radiative balance is not perfectly achieved level by level. However, variations induced in these rates by compositional differences are expected to be much less model-dependent, and hereafter we will only consider the *ratios* of the north to south cooling or heating rates rather than their absolute values.

Figure 4 shows the ratio of the northern cooling rate profile to the southern one for different atmospheric compositions (gas/haze) in the north. In all cases, the atmospheric model (temperature, gas, haze) used for the southern region is that yielding the best fitting of the corresponding IRIS spectrum. It is then possible to assess how the north-to-south variations in temperature, gas, and haze respectively affect the cooling rate profiles.

The curve labeled G_SH_S in Fig. 4 shows the cooling rate ratio derived when the same gas + aerosol model (corresponding to the best fit for the southern selection)

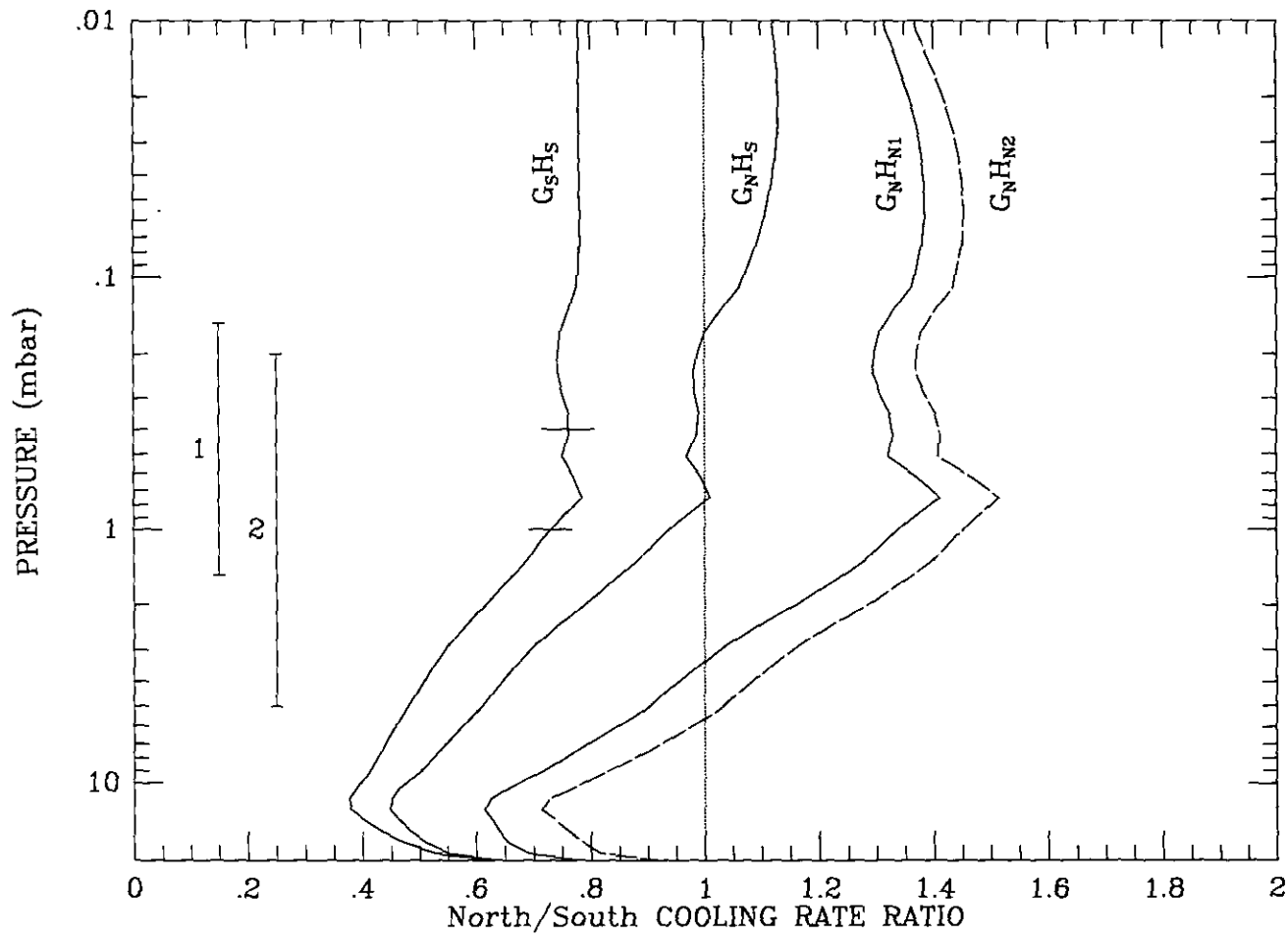

FIG. 4. Ratios of the north-to-south cooling rate profiles calculated for different atmospheric models in the north. (G_SH_S) was calculated assuming the same gas and haze model as at the southern location. In (G_NH_S), the enrichment in gas mixing ratios in the north was taken into account. Curves (G_NH_{N1}) and (G_NH_{N2}) further account for the enhancement in haze optical depth observed in the north, according to two different models (see text). The vertical regions over which information on the temperature is available are indicated (1 and 2). The formal error bars on the cooling rate ratio due to the 1 SD uncertainty on temperatures are plotted.

is used for the two locations. This calculation indicates the difference in the cooling rates due to temperature differences only. We find that, in the northern region, the cooling rates averaged over the pressure ranges 0.15–1.5 and 0.2–5 mbar would be 25 to 30% lower than in the warmer southern region, if the infrared opacity sources were the same.

In a second step, we have kept the same southern aerosol model but included the northern gas model having enriched concentrations for most species. Curve G_NH_S in Fig. 4 shows the 50°N-to-53°S cooling rate profile ratio calculated for this hybrid model. A comparison between Curves G_SH_S and G_NH_S indicate that taking into account the difference in gas concentrations yields an increase by about 30% in the cooling rates in the atmospheric layers probed by IRIS. More precisely, the cooling rate ratios averaged over the regions 0.15–1.5 mbar and 0.2–5 mbar are 0.97 and 0.88 respectively (to be compared to 0.75 and 0.68 when the same gas + haze southern model is used for the two locations). This means that, under the assumption of radiative equilibrium, the differences in gas composition alone could account for more than $\frac{2}{3}$ of the observed differences in stratospheric temperatures, if the solar heating were the same in both hemispheres (assuming here that the change in the cooling rate ΔK_c is proportional to the change in temperature ΔT to first order).

Finally, we computed the cooling rate profile for the northern location using the atmospheric model (gas and haze) offering the best fit with the corresponding IRIS spectrum. Using the nominal haze model (H_{N1}) described above, the larger particle opacity at northern latitudes produces an increase in the cooling rate profile of ~40% in the pressure range of interest. The ratio of the north-to-south cooling rates now reaches 1.33 and 1.23 in the regions 0.15–1.5 and 0.2–5 mbar, respectively. When the alternate northern haze model (H_{N2}) is used, an even larger increase in the cooling rate is found (the average north-to-south ratio is 1.42 and 1.34 in the two pressure ranges). The effect due the haze opacity enhancement is thus larger than that due to the enrichment in emitting gases.

Globally, moving from the atmospheric model relevant to the south to the northern one yields an increase in the cooling rates of at least 80% in the regions where temperature information is available. This is about twice the differences in the cooling rates arising solely from the north-to-south asymmetry in temperature (Fig. 4). At this point, we can conclude that the enhancement in the concentrations of infrared emittors at northern latitudes could easily account for the colder temperature profile observed there. This effect alone would actually cause a temperature contrast roughly twice as large. However, the north-to-south asymmetry in the haze structure also implies an asymmetry in the heating rate profiles. It is thus now necessary to estimate the magnitude of the latter effect to complete our radiative budget of the stratosphere at the two latitudes.

4. HEATING RATE CALCULATIONS

In the *Voyager* images of Titan the northern hemisphere was about 20% darker than the southern hemisphere in the violet (370–450 nm) and blue (430–530 nm) channels and about 15% darker in the green (520–600 nm) channel (Sromovsky *et al.* 1981). This is thought to be due to changes in the optical properties or concentration of the stratospheric haze. This north–south asymmetry likely accounts for most of the seasonal variations in Titan's geometric albedo as observed from the Earth (Lockwood *et al.* 1986). Recent observations of Titan by the Hubble Space Telescope, half an orbital period later than *Voyager*, show that the hemispheric contrast has reversed at the wavelengths of the *Voyager* filters—as expected if the variations are due to seasonal changes in the haze (Caldwell *et al.* 1992). The stratospheric haze on Titan controls the absorption of solar energy particularly for wavelengths less than 1 μm (McKay *et al.* 1989) and hence changes in the haze must be considered in our comparison of the radiative balance between northern and southern midlatitudes.

First we determine the change in solar heating associated with a change in the visible absorbance of the haze particles. Courtin (1992) has shown that the hemispheric asymmetry at visible wavelengths is consistent with a change in the absorbance of the haze particles by a factor of ~1.4, independent of wavelength. The absorbance would have been 1.4 times higher in the northern, darker hemisphere than in the southern hemisphere. The optical properties of the haze in Courtin (1992) are taken as a constant (nominally $\frac{3}{4}$ (McKay *et al.* 1989)) times the optical properties of organic material produced in laboratory simulations of Titan (Khare *et al.* 1984). This change in the optical properties provides one possible explanation for the *Voyager* results. Presumably the change in IR opacity would also be caused by a change in optical properties—a factor of 2.2 increase. It is unclear what compositional change could produce an increase of 1.4 and 2.2 in the visible and infrared absorption, respectively.

An alternate explanation that would be consistent simultaneously with the asymmetry in both the visible and the IR opacities would be a change in the column mass of the haze. If the optical properties of the haze are constant then more haze will result in a darkening in the visible wavelength seen by *Voyager* where the haze is an efficient absorber (see Fig. 4 of McKay *et al.* 1989) and will also increase the opacity in the infrared which is proportional to the column mass. Sromovsky *et al.* (1981) first proposed that the north–south contrast in the visible

albedo could result from differences either in the composition or in the optical depth of the aerosols, both of which could be indirectly produced by circulation currents. Pollack *et al.* (1980) proposed that changes in mass production rate of haze material could explain the seasonal variations in geometric albedo, but Hutzell *et al.* (1993) showed that time-dependent calculations cannot reproduce these variations with only changes in production rate and that transport of haze material had to be considered.

The IR opacity data (Table I) suggest that the mass must increase by a factor of 2.2 in the northern hemisphere with respect to the southern hemisphere. A twofold increase in mass production rate or column mass has also been suggested to explain the variation in the visible albedo (Pollack *et al.* 1980, Sromovsky *et al.* 1981, Hutzell *et al.* 1993). In a manner similar to increased production, vertical winds can also change the column mass and hence explain the variability in the geometric albedo (Toon *et al.* 1992). In both cases the effective change that alters the albedo is the size of the particles at the altitude corresponding to optical depth unity. The similarity between including a vertical wind and increasing the mass production is demonstrated in Fig. 10b of Toon *et al.* (1992). However, Courtin (1992) has pointed out that while the magnitude of the albedo change expected from a change in the mass production rate is in agreement with the visible observations of *Voyager*, the observations rise less steeply with wavelength than predicted. Toon *et al.* (1992) found a similar disagreement with models which include a vertical wind. We find that the change in the visible albedo as a function of wavelength for a doubling of the number of haze particles is similar to that obtained from a change in mass production rate and includes this slight disagreement with the data. Such a doubling also yields a reasonable approximation to the optical depth vertical profile obtained by Toon *et al.* (1992) for the main haze layer. We conclude that a factor of 2 increase in the haze amount provides a plausible, albeit imperfect, explanation for both the visible and infrared asymmetries. For this reason, we also considered an increase of the haze mass as a second possible explanation for the *Voyager* results.

Thus we considered two possible causes of the hemispherical asymmetry at the time of the *Voyager* observations: (1) an increase in the absorbance in the northern hemisphere by a factor of 1.4 and (2) a doubling of the number density of the haze particles in the northern hemisphere. In both cases all other microphysical properties of the haze are held constant. We used the microphysical haze model and radiative transfer scheme of McKay *et al.* (1989). Calculations include insolation conditions corresponding to diurnal averages for 50° latitude at equinox.

The "standard" haze model used at 53°S is the nominal model of McKay *et al.* (1989) in which the number of particles has been multiplied by 0.8 to account for the lower IR opacity in the south with respect to the equator (Table I). The corresponding heating rate is displayed in Fig. 3. Figure 5 shows the ratio of "perturbed" heating rate profiles to the standard case assumed to be representative of the south. Curve (A) shows the heating rate ratio that results from an increase in the absorbance by a factor of 1.4 while Curve (B) shows the result of doubling the number of the haze particles. In both cases the heating rates in the stratosphere increase. At 0.4 mbar the increase in heating is about 15% for a change in absorbance and about 75% for a doubling of the particles. At 1 mbar the corresponding values are 12 and 60%. Averaged over the ranges 0.15–1.5 and 0.2–5 mbar, the increases are 15 and 12% in Case (A), and 72 and 57% in Case (B).

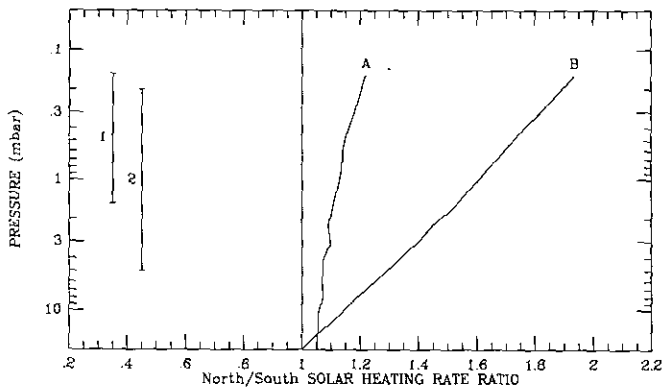

FIG. 5. Ratios of the north-to-south heating rate profiles calculated for two different haze models at 50°N. In both cases, the heating profile at 53°S is that displayed in Fig. 3. Profile (A) corresponds to an increase in the material absorbance by a factor of 1.4, and Profile (B) to a doubling of the particle density in the northern region.

We also investigated the sensitivity of these calculations to changes in the methane mixing ratio, still assumed to be the same at both latitudes. Cases were run for concentrations of 0.5 and 5% which represent realistic bounds of the actual abundance in the stratosphere (e.g., Lellouch *et al.* 1989). Models with a 0.5% mixing ratio are virtually identical to our nominal case (a 2% abundance). Absolute heating rates slightly increase when a 5% abundance is used, but the north–south ratios for Case B change by less than 10% in the whole region 0.15 to 5 mbar. The uncertainty in the CH_4 abundance thus appears to be negligible compared to other uncertainties such as those in the haze model.

5. DISCUSSION

Radiative-convective models of Titan's atmosphere (Samuelson 1983, McKay *et al.* 1989) provide a close match of the thermal profile derived from *Voyager* radio observations near the equator (Lindal *et al.* 1983). This general agreement strongly suggests that the stratosphere

of Titan, which is firmly stable against vertical convection, is governed chiefly by radiative processes. This is also supported by our calculations of the heating and cooling rate profiles based on models of the gas and haze opacity which reproduce the *Voyager* data near 53°S (Fig. 3). The two profiles fairly well agree in the atmospheric region where temperatures can be reliably retrieved from IRIS measurements (0.15–5 mbar). Radiative balance is thus achieved in our calculations to a good approximation.

Meridional temperature gradients are the result of the season-dependent insolation, the horizontal distribution of opacities for solar and thermal radiation, and the general circulation driven by the solar forcing. In this study, we investigated how the asymmetry in the solar and IR opacities affect the radiative equilibrium field by assessing the heat budget at two latitudes symmetric with respect to the equator (≈50°N and S).

Despite lower temperatures, the cooling rate profile at northern latitudes (50°N) appears to be larger than that at symmetric southern latitudes (53°S) because of enhanced concentrations of efficient infrared emittors (gas and haze particles). We found that the difference amounts to an average of 33 to 42% over the pressure range 0.15–1.5 mbar, and 23 to 34% for the interval 0.2–5 mbar, depending on the assumed spectral characteristics of the haze.

On the other hand, the lower visible albedo of Titan's northern hemisphere implies that the solar heating rates in the stratosphere are larger at northern latitudes than at symmetric locations in the south (having similar insolation conditions at the *Voyager* encounter time). The darker appearance of the northern hemisphere can be reproduced assuming an increase by a factor of 1.4 in the absorbance of the haze particles linked to a change in their chemical composition (Courtin 1992). The existence of such a compositional change seems reasonable since the composition of the gaseous atmosphere itself appears to strongly vary from one hemisphere to the other (Table I). Nitriles and hydrocarbons are likely to be precursors of Titan's organic haze, and the variation in their relative abundances could well cause a variation in the haze composition. Haze models with this higher absorbance produce an average increase in the solar heating rates of 15 and 12% in the regions 0.15–1.5 and 0.2–5 mbar (Case A). This variation is less than the difference in the cooling rates at the two locations. It means that the north/south asymmetry in gas and particle composition is not only capable of accounting for the observed asymmetry in the temperature field, but even tends to produce an even larger temperature contrast.

The lower brightness in the northern hemisphere could alternately be explained by a twofold increase in the particle number density, although the spectral dependence of the visible albedo is less well reproduced in this case (Courtin 1992). The solar heating rates are then 1.72 and 1.57 times those for the nominal number densities in the regions 0.15–1.5 and 0.2–5 mbar (Case B). This is significantly larger than the north/south ratio of the cooling rates. In this less likely case, the change in the atmospheric composition could not thus explain the whole observed temperature difference. From a comparison between Fig. 4 (G_SH_S and G_NH_{N1}, G_NH_{N2}) and 5 (B), we estimate that these compositional differences would only account for 10 to 60% of the temperature contrast in the range 0.15 to 5 mbar (assuming that changes in cooling rates are proportional to first order to temperature changes).

We conclude that north-to-south compositional changes are very likely capable of sustaining the observed north-to-south temperature gradient under radiative equilibrium conditions. In our nominal models for the infrared (G_NH_{N1}) and the visible (A), the variations in the gas and haze composition would produce an even larger temperature contrast, while in the least favorable, less likely, case (Profiles G_NH_{N1} and B), they would account for 10 to 30% of it. Model uncertainties are clearly large enough so that heat transport may play a significant role in the observed temperature asymmetry. Our study only demonstrates that radiative terms in the heat balance are not symmetric with latitude, and that the asymmetry is consistent with that in the temperature field; dynamical transport terms may still be an important contribution to the energy budget.

We have shown that the hemispheric asymmetry in infrared and solar opacity sources plays a key role in the asymmetry of the temperature field. Although, as emphasized by Flasar and Conrath (1990), the adiabatic cooling and heating associated with the planetary circulation could in principle cause a temperature asymmetry in the right direction, we believe that this asymmetry has mainly a radiative origin. Titan's temperature field would then represent the radiative equilibrium field and not lag behind it. It would still lag behind the solar heating mainly because of "chemical" rather than dynamical inertia. Yung (1987) proposed that the enrichment in nitriles observed at high northern latitudes was due to the low level of insolation in winter protecting these molecules from UV photolysis in the stratosphere once they are formed in the upper atmosphere and transported downward. Chemical time constants may be long enough to have prevented significant depletion of the high concentrations in nitriles and most hydrocarbons at the epoch of the *Voyager* encounter. If this idea is correct, the lag of the temperature field would indirectly result from long chemical time scales rather than a long dynamical time scale.

As a consequence of the present study, we expect that purely dynamical models which assume a symmetric meridional distribution of opacity about the equator will un-

derestimate the hemispheric asymmetry in stratospheric temperatures at equinox. Obviously, dynamical models incorporating a seasonally varying asymmetry in the distribution of opacity sources would be worth being developed in the future. This is however difficult, as the origin of the spatial and temporal variations of the gas and haze abundances is far from being fully understood. Observations by the *Cassini/Huygens* probe in 2004, at a season different from that at *Voyager*, will definitely help understanding the complex seasonal behavior of Titan's atmosphere.

REFERENCES

CALDWELL, J., C. C. CUNNINGHAM, D. ANTHONY, H. P. WHITE, E. J. GROTH, H. HASAN, K. NOLL, P. H. SMITH, M. G. TOMASKO, AND H. A. WEAVER 1992. Titan: Evidence for seasonal change—A comparison of Hubble Space Telescope and Voyager images. *Icarus* **96,** 1–9.

COURTIN, R. 1988. Pressure-induced absorption coefficients for radiative transfer calculations in Titan's atmosphere. *Icarus* **75,** 245–254.

COURTIN, R. 1992. Titan's UV albedo: Observations and modeling. In *Symposium on Titan,* pp. 59–67. ESA SP-338.

COUSTENIS, A., B. BÉZARD, AND D. GAUTIER 1989. Titan's atmosphere from Voyager infrared observations. I. The gas composition of Titan's equatorial region. *Icarus* **80,** 54–76.

COUSTENIS, A., B. BÉZARD, D. GAUTIER, A. MARTEN, AND R. SAMUELSON 1991. Titan's atmosphere from Voyager infrared observations. III. Vertical distributions of hydrocarbons and nitriles near Titan's north pole. *Icarus* **89,** 152–167.

COUSTENIS, A., AND B. BÉZARD 1994. Titan's atmosphere from Voyager infrared observations. IV. Latitudinal variations of temperature and composition. Submitted.

FLASAR, F. M., R. E. SAMUELSON, AND B. J. CONRATH 1981. Titan's atmosphere: Temperature and dynamics. *Nature* **292,** 693–698.

FLASAR, F. M., AND B. J. CONRATH 1990. Titan's stratospheric temperatures: A case for dynamical inertia? *Icarus* **85,** 346–354.

HUTZELL, W. T., C. P. MCKAY, AND O. B. TOON 1993. Effects of time-varying haze production on Titan's geometric albedo. *Icarus* **105,** 162–174.

KHARE, B. N., C. SAGAN, E. T. ARAKAWA, F. SUITS, T. A. CALLCOTT, AND M. W. WILLIAMS 1984. Optical constants of organic tholins produced in a simulated Titanian atmosphere: From soft X-ray to microwave frequencies. *Icarus* **60,** 127–137.

LELLOUCH, E., A. COUSTENIS, D. GAUTIER, F. RAULIN, N. DUBOULOZ, AND C. FRÈRE 1989. Titan's atmosphere and hypothesized ocean: A reanalysis of the Voyager 1 radio-occultation and IRIS 7.7 μm data. *Icarus* **79,** 328–349.

LINDAL, G. F., G. E. WOOD, H. B. HOTZ, D. N. SWEETNAM, V. R. ESHLEMAN, AND G. L. TYLER 1983. The atmosphere of Titan: An analysis of the Voyager 1 radio occultation measurements. *Icarus* **53,** 348–363.

LOCKWOOD, G. W., B. L. LUTZ, D. T. THOMPSON, AND E. S. BUS 1986. The albedo of Titan. *Astrophys. J.* **303,** 511–520.

MCKAY, C. P., J. B. POLLACK, AND R. COURTIN 1989. The thermal structure of Titan's atmosphere. *Icarus* **80,** 23–53.

POLLACK, J. B., K. RAGES, O. B. TOON, AND Y. L. YUNG 1980. On the relationship between secular brightness changes of Titan and solar variability. *Geophys. Res. Lett.* **7,** 829–832.

RAGES, K., AND J. B. POLLACK 1980. Titan aerosols: optical properties and vertical distribution. *Icarus* **41,** 119–130.

SAMUELSON, R. E. 1983. Radiative equilibrium model of Titan's atmosphere. *Icarus* **53,** 364–387.

SAMUELSON, R. E., AND L. A. MAYO 1991. Thermal infrared properties of Titan's stratospheric aerosol. *Icarus* **91,** 207–219.

SROMOVSKY, L. A., V. E. SUOMI, J. B. POLLACK, R. J. KRAUSS, S. S. LIMAYE, T. OWEN, H. E. REVERCOMB, AND C. SAGAN 1981. Implications of Titan's north–south brightness asymmetry. *Nature* **292,** 698–702.

TOON, O. B., C. P. MCKAY, R. COURTIN, AND T. P. ACKERMAN 1988. Methane rain on Titan. *Icarus* **75,** 255–284.

TOON, O. B., C. P. MCKAY, C. A. GRIFFITH, AND R. P. TURCO 1992. A physical model of Titan's aerosols. *Icarus* **95,** 24–53.

YELLE, R. V. 1991. Non-LTE models of Titan's upper atmosphere. *Astrophys. J.* **383,** 380–400.

YUNG, Y. L., M. ALLEN, AND J. P. PINTO 1984. Photochemistry of the atmosphere of Titan: Comparison between model and observations. *Astrophys. J. Suppl.* **55,** 465–506.

YUNG, Y. L. 1987. An update of nitrile photochemistry on Titan. *Icarus* **72,** 468–472.